ACES
doi.org/10.1002/asia.202500792
CHEMISTRY
AN ASIAN JOURNAL
Research Article
www.chemasianj.org

共同一作，贡献度60%

Titanium Oxynitride-Supported Iridium Electrocatalysts for Efficient and Durable Acidic Oxygen Evolution Reaction

Jian Wei Guo†,[a] Hao Yang Lin†,[a] Huan Wang,[a] Fang Xin Mao,*[a] Shuang Yang,[a] Peng Fei Liu,*[a] and Hua Gui Yang[a]

Iridium-based materials are state-of-the-art electrocatalysts for the acidic oxygen evolution reaction (OER). In this work, an efficient low-iridium electrocatalyst is successfully anchored on a typical titanium oxynitride support, achieving an overpotential as low as 278 mV and robust stability over 1000 h at 10 mA cm^{-2} in 0.5 M H_2SO_4. It is discovered that high valence Ir(VI) sites can be in situ formed under the interaction of support during OER procedure, accounting for the superior performance. We show that rational design of support can realize activity and stability enhancement, demonstrating a feasible approach for acidic OER electrocatalysts.

1. Introduction

Water electrolysis powered by the sustainable electrical energy is a nearly perfect technology for production of green hydrogen and is crucial to global decarbonization efforts.[1] Oxygen evolution reaction (OER), anodic half reaction of electrochemical water splitting, suffers from sluggish kinetics for its four-electron transfer procedure and governs the efficiency of overall reaction.[2] Furthermore, harsh acidic conditions would be generated in proton exchange membrane (PEM) water electrolysis, requiring a basic qualification of corrosion-resistant for materials to catalyze OER process. Currently, iridium (Ir) oxides are the only practical electrocatalyst which can tolerate the operating conditions in PEM electrolyzer.[3] Unfortunately, scarce storage and high cost of Ir have become essential challenge for large-scale development of PEM electrolyzer.[4] Significantly enhancing the activity of the Ir catalyst and reducing its consumption have become the key issues that urgently need to be addressed in this field.

Maximizing the atomic utilization of Ir would provide a viable strategy to realize a balance catalytic activity and cost. To disperse Ir active sites, stable support is demonstrated tool for immobilizing them and adjusting activity.[5] Strong support is expected with good conductivity to facilitate electron and charge transfer during OER between the electrode, catalyst, and electrolyte.[6] Titanium compounds such as TiO_2 have been used as multiple heterogeneous catalyst support for its high physical and chemical stability.[7] TiO_2-supported crystalline IrO_2 catalysts (Elyst Ir75 0480 Umicore, 75 wt.% Ir) is reported a commercial supported materials.[8] However, a *n*-type semiconductor of titania, band gap is as large as 3.2 eV, could perform deficient electron conductivity for electrocatalysis.[9] More than the insert matrix for active sites, functional supports such as reducible ones would enhance the oxidation of metal centers and improve the kinetics of OER, leading to facilitate formation of intermediates.[10] Heteroatom doping, including of metal and non-metal atoms, titanium suboxide, and shaped TiO_2, etc., methods have been reported to improve the electrocatalytic property.[11] Huge potential lies in the titanium-supported Ir catalysts for an efficient and durable acidic OER process.

Titanium oxynitride intermediate between the insulating TiO_2 and metallic TiN, could be regulated progressively band structure for the suitable stability and conductivity property.[12] It had been reported that TiN could effectively loaded IrO_2@Ir uniformly on surface and prevent the active Ir from oxidative dissolution. However, only few hours stability was reported even with high Ir content 60 wt.%.[13] Based on the most stable structure of TiO_2, O atoms are favorable to incorporate and substitute N atoms in TiN.[14] In this work, thermal oxidization of commercial nanostructured TiN has been implemented to create suitable support to load iridium catalyst. We regulate the content of N and O elements and synthetically study the catalyst-support effect for acidic OER performance. High oxidation state of Ir(VI) active sites are demonstrated in an electrochemical procedure, which could be facilitated by the support interaction. Adsorption oxygen evolution mechanism has been verified by the in situ synchrotron radiation infrared measurement. The resultant optimal titanium oxynitride support Ir electrocatalyst can motivate efficient and durable OER process, needing only the overpotential of 278 mV to achieve 10 mA cm^{-2} and continuously operating for more than 1000 h in acidic electrolyte. The mass activity of Ir/TiN-450 presents as high as 256 A g_{Ir}^{-1}@1.53 V and 2244 A g_{Ir}^{-1}@1.58 V (versus reversible hydrogen electrode, RHE).

[a] J. W. Guo†, H. Y. Lin†, H. Wang, F. X. Mao, S. Yang, P. F. Liu, H. G. Yang
Key Laboratory for Ultrafine Materials of Ministry of Education, Shanghai Engineering Research Center of Hierarchical Nanomaterials, School of Materials Science and Engineering, East China University of Science and Technology, 130 Meilong Road, Shanghai 200237, China
E-mail: fxmao@ecust.edu.cn
pfliu@ecust.edu.cn

[†] Both authors contributed equally to this work.

Supporting information for this article is available on the WWW under https://doi.org/10.1002/asia.202500792

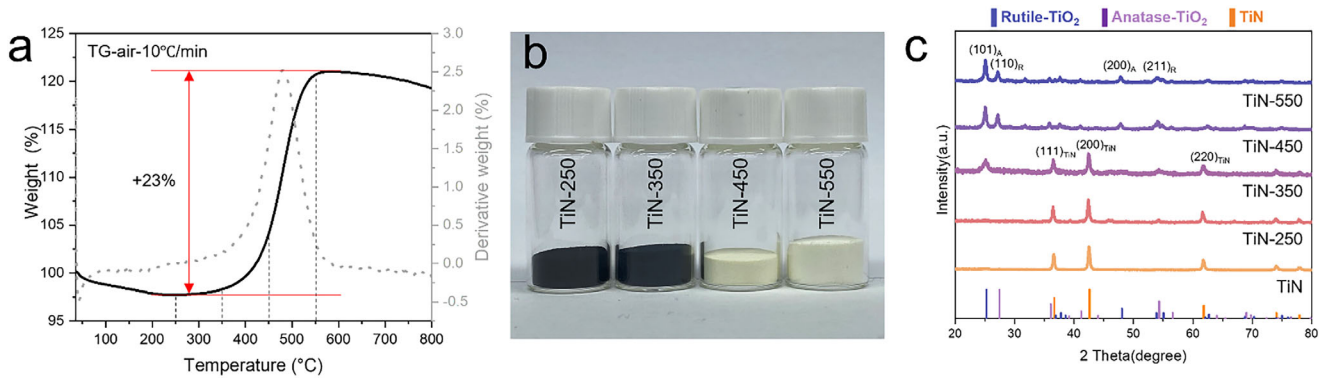

Figure 1. a) TGA curves of the TiN support in the air atmosphere. b) Digital photograph of the samples thermo-treated at serial temperatures. c) XRD patterns of the samples in contrast with the standard titanium oxides and nitride.

2. Results and Discussion

Titanium oxynitride supports were prepared by one-step oxidization of commercial TiN nanoparticles under air atmosphere at the serial temperature (250 °C, 350 °C, 450 °C, and 550 °C). Different phase structure (TiN-*X*, where *X* represents the thermal treatment temperature) could be formed on account of oxidization degree. Thermogravimetric analysis (TGA) in Figure 1a showed the weight changing behavior that oxidization of TiN occurred at the temperature of larger than 250 °C and complete oxidization might be achieved around 550 °C. In the oxidizing process, the largest weighting rate occurred at 450 °C, demonstrating the fast gas-solid thermal reaction. That only 23% weighting by oxidization reaction, less than the theory value of 29% for transforming TiN to TiO_2, proved residual N element in the final product. The digital photos (Figure 1b) clearly exhibited that the color of TiN particles turned from black to blue-black, faint yellow, and white along with increasing treatment temperature. As shown in Figure 1c, X-ray diffraction (XRD) results demonstrated that the observable phase transfer generated after treating at a higher temperature than 350 °C, in which feature anatase TiO_2 and TiN peaks existed in the pattern of TiN-350. For TiN-450 and TiN-550, a hybrid matrix could be verified with titanium oxides of rutile and anatase phases, consisting of small quantity of TiN. Therefore, titanium oxynitride supports can be obtained by the simple oxidization treatment of titanium nitride.

Nanostructured iridium (Ir) species were immobilized onto support surface by the solvothermal polyalcohol reduction method. As shown in Figure 2a, high-angle annular dark-field imaging-scanning transmission electron microscope (HAADF-STEM) image of Ir/TiN-450 presented a bright outline on the nanoparticles, and uniform dispersion of Ir, Ti, O, and N elements. The Ir/TiN-*X* samples showed uniform nanoparticles morphology with size about 50 nm by the scanning electron microscope (SEM). The XRD Ir/TiN-*X* samples revealed that the supports phase could remain in the loading Ir process (Figures S1 and S2). Samples' element analysis was listed in Table S1. N and O elements proportions were analyzed by X-ray energy dispersive spectrometer (EDS) for Ir/TiN, Ir/TiN-250, Ir/TiN-350, Ir/TiN-450, and Ir/TiN-550 samples. Successful loading of Ir onto supports can be achieved by this method. As shown in Figure S3, the proportion of N/(N + O) reduced from ~90% (Ir/TiN) to ~18% (Ir/TiN-550) because of that partial N would be replaced by O during thermal procedure of TiN supports.

The magnified image presents that ultrafine Ir nanoparticles (Ir NPs) are located densely on the TiN-450 supports, and their particle sizes were about 2 ~ 3 nm (Figure 2b). The fast Fourier transform (FFT) image of inset demonstrated the typical diffraction ring of Ir, diffraction spots of TiO_2 (101) and TiO_2 (030) facets, marked with yellow cycles in the picture. High crystallinity ultrafine Ir NPs loaded on the TiO_2 nanocrystal by tight interface (Figure 2c). Typical diffraction spots of Ir (1–1–1) and Ir (200) are shown in the magnified box for Ir NPs region. Bright field-STEM (BF-STEM) image of Ir/TiN-450 in Figure S4 provided the further evidence that atomic-level interfacial adhesion between Ir NPs and TiN-450 supports.

X-ray absorption fine structure (XAFS) characterization was implemented to explore the electronic structure and local coordination configuration of materials. As shown in Figure 2d, X-ray absorption near edge spectra (XANES) of Ir L_3-edge exhibited similar white peaks of Ir/TiO_2, Ir/TiN, and Ir/TiN-450, located between ones of Ir foil (Ir^0) and IrO_2 (Ir^{4+}) references. Extended X-ray absorption fine structure (EXAFS) showed a larger Ir—O and shorter Ir—Ir distances in Ir/TiO_2, Ir/TiN, and Ir/TiN-450 compared with that of IrO_2. The bond of Ir-O/N could be formed between Ir nanoparticles and supports, leading to a strong interaction. A distorted iridium oxides structure could be affirmed for the supported samples, which may be leaded by the strong catalyst-support effect. X-ray photoelectron spectra (XPS) showed that more metallic state Ir could be formed in titanium oxide and oxynitride supports than that of Ir/TiN (Figure S5). XPS spectra of Ti 2p were also collected as Figures S6, and oxidized Ti could be observed for the thermal treating samples.

The acidic OER performance of samples were evaluated in a dilute sulphuric acid electrolyte (0.5 M H_2SO_4). As shown in Figure S7, linear sweep voltammetry (LSV) curves present the OER catalytic activity of Ir/TiN-*X* samples, in which Ir/TiN-450 performed a better activity than the others. The support

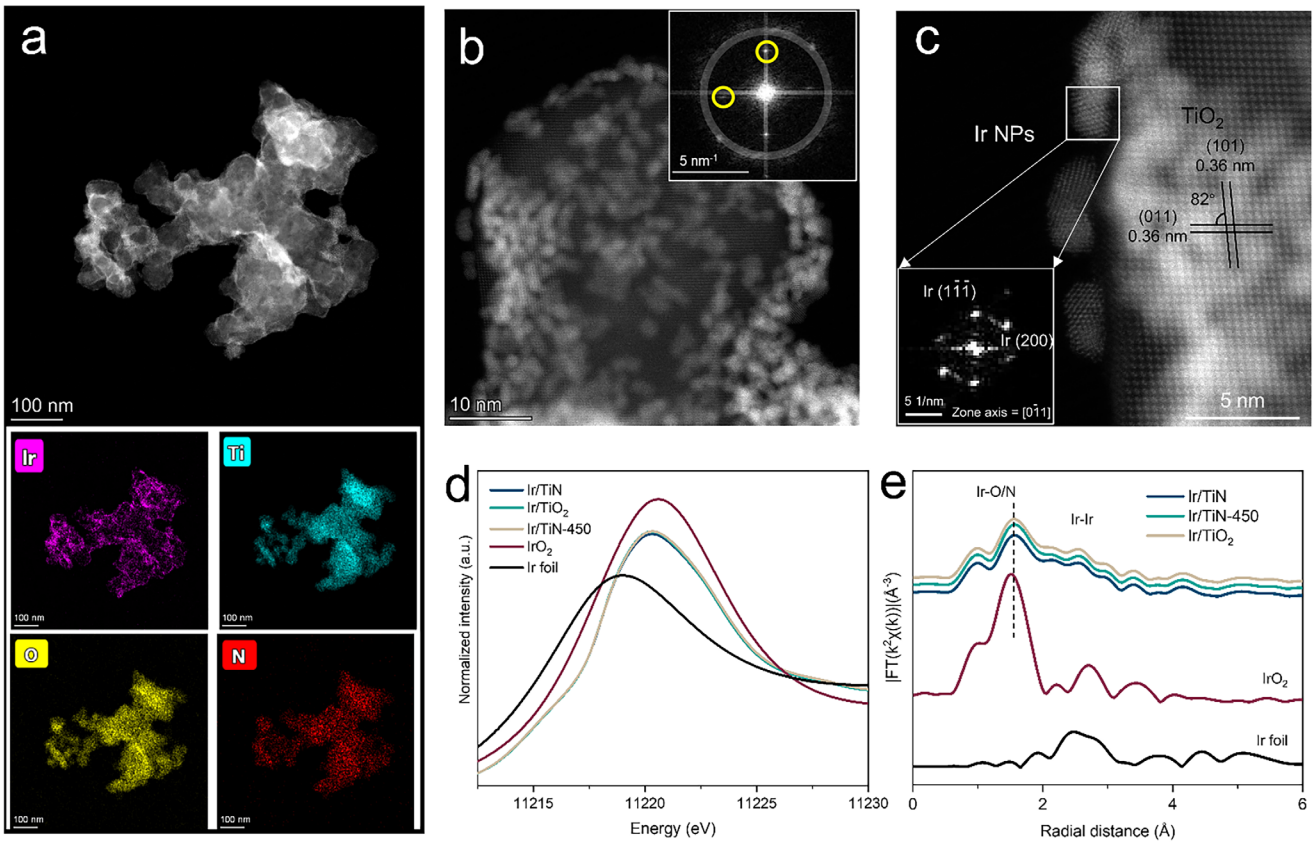

Figure 2. a) HAADF-STEM image of Ir/TiN-450 sample and the corresponding element mappings of Ir, Ti, O, and N. b) HAADF-STEM image of Ir/TiN-450 sample, showing that iridium pieces uniformly disperse at the support surface. The inset of FFT image demonstrates the characteristic diffraction spots of TiO_2 and the diffraction ring of Ir. c) HAADF-STEM image with the atomic level resolution. FFT pattern of Ir NPs is enlarged in the marked box. d) and e) XAFS spectra of Ir/TiO_2, Ir/TiN, Ir/TiN-450, and the control samples.

could play vital role toward the catalytic sites. Based on the Ir contents in samples, mass activity could be evaluated that 256 A g_{Ir}^{-1} @1.53 V and 2244 A g_{Ir}^{-1} @1.58 V for Ir/TiN-450 (Figure S8). Electrochemical active area (ECSA) was estimated by electrical double-layer capacitance (C_{dl}) using cyclic voltammetry (CV) method. As shown in Figures S9 and S10, Ir/TiN-450 performed a larger ECSA and acts as an optimized candidate electrocatalyst.

The systematic materials were measured to study the support effect. As shown in Figure 3a, as-prepared materials performed better OER activity than the commercial Umicore (Ir/TiO_2, 75 wt.%) catalyst. Compared with as-prepared Ir NPs, Ir/TiN-450, Ir/TiN, and Ir/TiO_2 samples exhibit the enhanced activities, proving that suitable supports and composition contribute to activity. Their OER activities ranked as Ir/TiN-450 > Ir/TiN > Ir/TiO_2 > Ir NPs > Umicore. That ECSA normalized LSV of Ir/TiN-450 and Ir NPs further verifies the support effect for activity enhancement (Figures S11, S12, and Table S2). The overpotential of Ir/TiN-450 at a current density of 10 mA cm^{-2} showed as low as 278 mV to achieve the current density of 10 mA cm^{-2}, dramatically less than that of commercial Umicore (370 mV) (Figure 3b). Good reproducibility of Ir/TiN-450 materials were demonstrated by three independent batch measurements (Figure S13). In comparison with the previous reports, as-synthesized Ir/TiN-450 exhibits the prominent performances (Table S3). Tafel slope and electrochemical impedance spectroscopy (EIS) had been supplemented to study the electrochemical properties of the materials. As shown in Figures 3c,d and S14, low Tafel slope of 48 mV dec^{-1} revealed the faster kinetics for Ir/TiN-450, which might benefit by the small electron transfer resistance. The fitted circuit parameters are listed in Table S4.

Ir leaching behaviors were detected by inductively coupled plasma mass spectrometry (ICP-MS) using Ir/TiN-450, Ir/TiO_2, Ir NPs samples. Under the galvanostatic of 10 mA cm^{-2} condition, Ir/TiN-450 occurred less Ir leaching than Ir NPs and Ir/TiO_2, though, fast leaching in the first hour for three samples (Figure 3e). Metallic Ir nanoparticles may dissolve through Ir(III) species formed during anodic oxidization procedure. Ir/TiN-450 leached less Ir species after 100 h electrolysis and performed a better stability. Long-term operation test of Ir/TiN-450 showed an excellent stability for 1000 h at a current density of 10 mA cm^{-2}, in which slight potential increasing as low as 8.4 μV h^{-1} (Figure 3f). LSV plots were also measured to confirm the performance change (Figure S15). Structural characterizations of Ir/TiN-450 after electrolysis could reveal robust anchoring on the support (Figure S16). In conclusion, Ir/TiN-450 was demonstrated with good catalytic activity and stability for acidic OER.

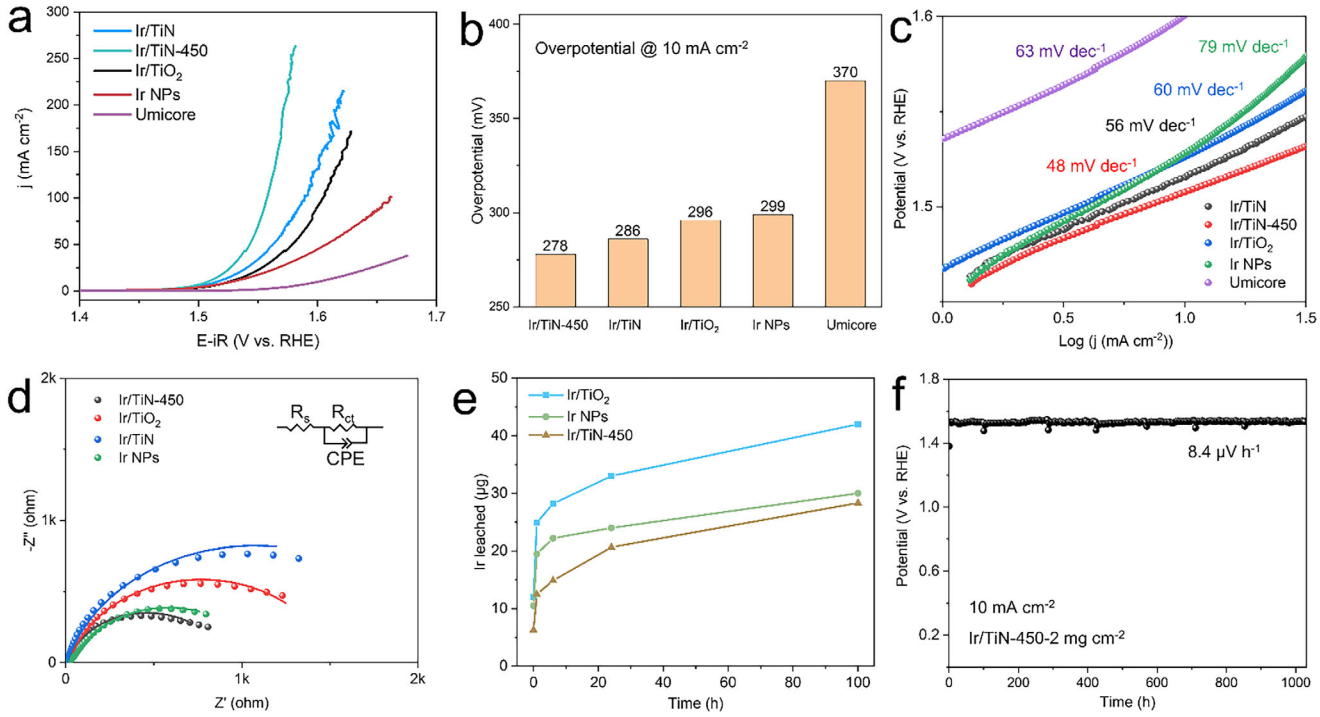

Figure 3. a) LSV curves of prepared samples and commercial contrasts to evaluate OER activity. b) Overpotential at the current density of 10 mA cm^{-2} and c) Tafel slope obtained from the corresponding LSV results. d) Nyquist plots of electrochemical impedance spectroscopy (EIS) for Ir/TiN-450, Ir/TiN, Ir/TiO_2, and Ir NPs. e) Ir leaching quantification curves of Ir/TiO_2, Ir NPs, and Ir/TiN-450 based on the catalytic time at the current density of 10 mA cm^{-2}. f) Galvanostatic stability curve of Ir/TiN-450 with a test time of more than 1000 h.

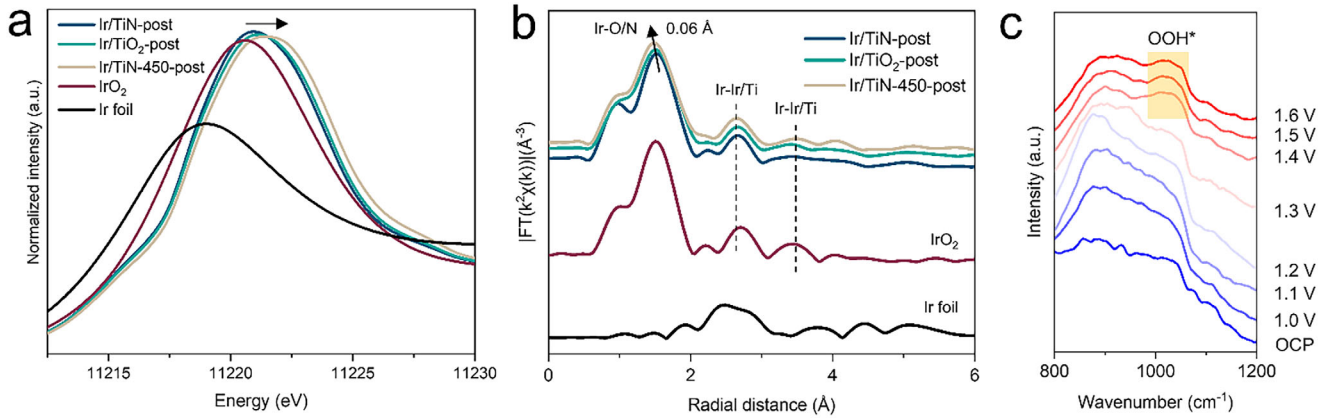

Figure 4. a) and b) XAFS spectra of Ir/TiO_2, Ir/TiN, and Ir/TiN-450 samples post-electrocatalysis process. c) In situ SRIR spectra of Ir/TiN-450 measured at the different applied potentials.

To understand the interaction of supports to the iridium species, local structure evolution was investigated by XAFS for Ir/TiO_2, Ir/TiN, and Ir/TiN-450 samples suffering the OER procedure, 100 h at a current density of 10 mA cm^{-2}. As shown in Figure 4a, white peaks of samples shifted toward high energy region and the intensities exceeded that of IrO_2, demonstrating that iridium can be oxidized with oxidized polarizing potential. Energy at white line of Ir/TiN-450-post was larger than Ir/TiN-post and Ir/TiO_2-post samples, indicating its higher oxidation state. In the second derivative curves (Figure S17), minimal point locating energy value could further illustrate this phenomenon. Referring the XANES of IrO_2 (Ir^{4+}), Ir(VI) active sites could be verified in Ir/TiN-450-post.[15] Abundant Ir(VI) central motifs endowed the highly active and stable OER sites for Ir/TiN-450-post.[16] EXAFS of Ir/TiN-450-post displayed a compressive Ir-O/N bond compared with that of Ir/TiN-post and Ir/TiO_2-post, which might be caused by the large electric charge interaction of Ir(VI) sites.[17] According to XPS spectra before and post catalysis, Ti 2p peaks shift toward the lower binding energy for Ir/TiN-450 (Figure S18), demonstrating that TiN-450 could become electron acceptor in the catalytic procedure.[18] This property of TiN-450 could facilitate the gen-

eration of Ir(VI) sites, and enhance the OER performance in contrast to TiO_2 support. In situ synchrotron radiation infrared (SRIR) characterization probed the reaction intermediate in OER progress. Signal of OOH* located at ~1030 cm^{-1} provided crucial evidence of the adsorption oxygen evolution mechanism on Ir/TiN-450.[19] Therefore, Ir/TiN-450 performed outstanding acidic OER performances due to its titanium oxynitride supported structure.

3. Conclusion

In summary, this work has reported an efficient titanium oxynitride supported iridium electrocatalyst by thermal treatment of the conductive titanium nitride precursor and followed uniform loading. Through characterization methods such as XRD, TEM, XPS, XAFS, and in situ electrochemical SRIR, the surface microstructure and electronic structure of the catalyst are systematically analyzed. The TiN-450 support is demonstrated as an electron acceptor during the OER process, accelerating the formation of high-valent and highly active centers of Ir(VI) in Ir/TiN-450 materials. The adsorption oxygen evolution mechanism has been verified based on the in situ SRIR result. Low overpotential of 278 mV at a current density of 10 mA cm^{-2} has been realized, maintaining this activity more than 1000 h. The study highlights a synthesis and modification method for low-Ir electrocatalysts, to further construct a low-Ir PEM electrolyzer with the reduced consumption.

4. Experimental Section

4.1. Materials

All the chemicals were used without further purification provided by the suppliers. Titanium nitride (TiN) and titanium oxide (TiO_2) nanoparticles were purchased from Macklin Inc. Hexachloroiridium acid hydrate ($H_2IrCl_6{\cdot}xH_2O$, 99.9%) was purchased from Alfa Aesar (China) Chemical Co., Ltd. Ethylene glycol ($HOCH_2CH_2OH$, AR), P123 and Nafion solution (5 wt.%) were provided by the Sigma-Aldrich (Shanghai) Trading Co.,Ltd. Sulfuric acid (95.0–98.0%) was purchased from Sinopharm Chemical Reagent Co., Ltd. Isopropanol ($(CH_3)_2CHOH$, AR) was purchased from Shanghai Lingfeng Chemical Reagent Co., Ltd. Ultrapure water was produced in the laboratory with an electrical resistivity larger than 18.2 MΩ cm.

4.2. Synthesis of the Samples

Synthesis of titanium oxynitride (TiN-*X*). The commercial TiN nanoparticles were calcined at serial temperature of 250 °C, 350 °C, 450 °C, and 550 °C in a muffle furnace. In the calcining process, the samples were treated for 2 h at the object temperature with a heating rate of 5 °C min^{-1}. and collected after natural cooling. TiN-*X* presents the sample obtained with corresponding parameter (*X* = temperature value).

Synthesis of Ir/TiN-*X*: Solvothermal polyalcohol reduction method was implemented to load iridium onto TiN-*X* supports surface. Typically, 40 mg TiN-*X* materials and 80 mg P123 were dispersed in 20 mL ethylene glycol by ultrasonic dispersing for 30 min in a three-neck flask. Hexachloroiridium acid hydrate (81.4 mg) was introduced into solution with continue dispersing for another 30 min. Heating the flask at 120 °C for 3 h in the oil bath under magnetic stirring, equipped with a reflux condensation during reaction. The samples were collected by the centrifugal washing with water and absolute ethyl alcohol, and were dried in a vacuum oven at 60 °C.

Synthesis of Ir/TiN: The similar procedure was carried out to prepare Ir/TiN like that of Ir/TiN-*X*, in which support materials were replaced by untreated TiN.

Synthesis of Ir/TiO_2: The similar procedure was carried out to prepare Ir/TiO_2 like that of Ir/TiN-*X*, in which support materials were replaced by commercial TiO_2.

Synthesis of Ir NPs: The Ir NPs sample was prepared by the same method, with the absence of support materials.

4.3. Characterizations

Thermogravimetric analysis was implemented using a PerkinElmer TGA 8000 analyzer heating from room temperature to 800 °C with rate of 10 °C min^{-1} under air atmosphere. The crystal structure of the samples was characterized by X-ray diffraction (XRD, D/max2550V) equipped with a monochromatic Cu K_α radiation source and a D8 Advanced diffractometer. Thermo Fisher Talos F200X and Thermo Fisher Themis Z electron microscope equipped with two aberration correctors were applied to measure the morphology structure of samples. XPS characterization was performed on a Thermo ESCALAB 250Xi equipped with monochromatic X-rays generated by Al K_α (1486.6 eV), in which the binding energy of the C 1s main peak was calibrated to 284.8 eV. X-ray absorption fine structure (XAFS) measurements were conducted at the BL14W1 beamline of the Shanghai Synchrotron Radiation Facility (SSRF) under operating conditions of 210 mA and 3.5 GeV. In situ electrochemical synchrotron radiation infrared spectroscopy (SRIR) tests were performed using a custom-built top-plate reflection infrared setup at the infrared beamline BL01B of the National Synchrotron Radiation Laboratory (NSRL) in China. The SRIR setup consisted of an infrared spectrometer (Bruker 66 V s^{-1}) with a KBr beam splitter, a liquid nitrogen-cooled MCT detector, and an infrared microscope (Bruker Hyperion 3000) equipped with a ×16 objective lens. This system provided a high resolution of 0.25 cm^{-1} in the range of 15–4000 cm^{-1}.

4.4. Electrochemical Measurements

Glassy carbon electrode (GCE, with a diameter of 3 mm) was drop-coating catalysts for performance test. 5 mg of catalyst powder was dispersed in 0.25 mL of isopropanol and 0.75 mL of deionized water, and then 40 µL of 5 wt.% Nafion solution was added. The suspension was dispersed in an ultrasonic machine for at least 60 min to obtain a uniformly dispersed catalyst ink. Then, 5 µL of the catalyst ink was carefully dripped onto the glassy carbon electrode using a micropipette (with a catalyst loading of 0.3538 mg cm^{-2}), and left to dry naturally. Three-electrode system was used with Pt counter electrode and Hg/Hg_2SO_4 reference electrode, equipped with electrolyte of 0.5 M H_2SO_4 solution. All electrochemical tests were implemented on a CHI660E workstation.

Acknowledgments

This work was financially supported by the Shanghai Pilot Program for Basic Research (22TQ1400100-12), and the Fundamental Research Funds for the Central Universities. The authors thank

the Frontiers Science Center for Materiobiology and Dynamic Chemistry and the National Synchrotron Radiation Laboratory (NSRL). The authors also thank the Shanghai Synchrotron Radiation Facility of BL14B1 (https://cstr.cn/31124.02.SSRF.BL14W1) for providing technical support and assistance in XAFS data collection.

Conflict of Interests

The authors declare no conflict of interest.

Data Availability Statement

The data that support the findings of this study are available from the corresponding author upon reasonable request.

Keywords: Iridium-based materials · Oxygen evolution reaction · Supports · Titanium oxynitride · Water splitting

[1] a) M. Chatenet, B. G. Pollet, D. R. Dekel, F. Dionigi, J. Deseure, P. Millet, R. D. Braatz, M. Z. Bazant, M. Eikerling, I. Staffell, P. Balcombe, Y. Shao-Horn, H. Schäfer, *Chem. Soc. Rev.* **2022**, *51*, 4583-4762; b) H. Sun, X. Xu, H. Kim, W. Jung, W. Zhou, Z. Shao, *Energy Environ. Mater.* **2023**, *6*, e12441.
[2] a) J. Song, C. Wei, Z.-F. Huang, C. Liu, L. Zeng, X. Wang, Z. J. Xu, *Chem. Soc. Rev.* **2020**, *49*, 2196-2214; b) E. Fabbri, T. J. Schmidt, *ACS Catal.* **2018**, *8*, 9765-9774.
[3] a) W. Shi, T. Shen, C. Xing, K. Sun, Q. Yan, W. Niu, X. Yang, J. Li, C. Wei, R. Wang, S. Fu, Y. Yang, L. Xue, J. Chen, S. Cui, X. Hu, K. Xie, X. Xu, S. Duan, Y. Xu, B. Zhang, *Science* **2025**, *387*, 791–796; b) M. van der Merwe, R. Garcia-Diez, L. Lahn, R. E. Wibowo, J. Frisch, M. Gorgoi, W. Yang, S. Ueda, R. G. Wilks, O. Kasian, M. Bär, *ACS Catal.* **2023**, *13*, 15427–15438; c) K. Zhang, X. Liang, L. Wang, K. Sun, Y. Wang, Z. Xie, Q. Wu, X. Bai, M. S. Hamdy, H. Chen, X. Zou, *Nano Res. Energy* **2022**, *1*, e9120032.
[4] a) M. Clapp, C. M. Zalitis, M. Ryan, *Catal. Today* **2023**, *420*, 114140; b) C. Mittelsteadt, E. Sorensen, Q. Jia, *Energy Fuels* **2023**, *37*, 12558–12569.
[5] L. Moriau, M. Smiljanić, A. Lončar, N. Hodnik, *ChemCatChem* **2022**, *14*, e202200586.
[6] a) S. Zaman, M. Khalid, S. Shahgaldi, *ACS Energy Lett.* **2024**, *9*, 2922–2935; b) A. Venugopal, L. H. T. Egberts, J. Meeprasert, E. A. Pidko, B. Dam, T. Burdyny, V. Sinha, W. A. Smith, *ACS Energy Lett.* **2022**, *7*, 1586–1593.
[7] S. Bagheri, N. Muhd Julkapli, S. Bee Abd Hamid, *Sci. World J.* **2014**, *2014*, 1-21.
[8] M. Bernt, C. Schramm, J. Schröter, C. Gebauer, J. Byrknes, C. Eickes, H. A. Gasteiger, *J. Electrochem. Soc.* **2021**, *168*, 084513.
[9] B. Kraeutler, A. J. Bard, *J. Am. Chem. Soc.* **1978**, *100*, 4317-4318.
[10] a) S. Roy, S. Roy, *ACS Appl. Nano Mater.* **2024**, *7*, 26534–26545; b) S. Roy, P. Dahiya, T. K. Mandal, S. Roy, *Dalton T* **2024**, *53*, 5484–5494.
[11] a) K. Chen, T. Shen, Y. Lu, Y. Hu, J. Wang, J. Zhang, D. Wang, *J. Energy Chem.* **2022**, *67*, 168–183; b) S. zhu, S. Yi, X. Zhang, L. Yu, Z. Jiang, X. Tang, S. Li, L. Li, Y. Wang, H. Tang, *Energy Fuels* **2025**, *39*, 6505–6516; c) Y. Qin, Y. Wang, R. Wen, L. Wang, M. Dou, F. Wang, *ACS Catal.* **2024**, *14*, 13915–13926.
[12] N. R. Mucha, J. Som, J. Choi, S. Shaji, R. K. Gupta, H. M. Meyer, C. L. Cramer, A. M. Elliott, D. Kumar, *ACS Appl. Energy Mater.* **2020**, *3*, 8366–8374.
[13] G. Li, K. Li, L. Yang, J. Chang, R. Ma, Z. Wu, J. Ge, C. Liu, W. Xing, *ACS Appl. Mater. Interfaces* **2018**, *10*, 38117–38124.
[14] a) J. Graciani, S. Hamad, J. F. Sanz, *Phys. Rew. B* **2009**, *80*, 184112; b) K. P. McKenna, *J. Appl. Phys.* **2018**, *123*, 075301.
[15] A. Li, S. Kong, K. Adachi, H. Ooka, K. Fushimi, Q. Jiang, H. Ofuchi, S. Hamamoto, M. Oura, K. Higashi, T. Kaneko, T. Uruga, N. Kawamura, D. Hashizume, R. Nakamura, *Science* **2024**, *384*, 666–670.
[16] R. A. Flores, C. Paolucci, K. T. Winther, A. Jain, J. A. G. Torres, M. Aykol, J. Montoya, J. K. Nørskov, M. Bajdich, T. Bligaard, *Chem. Mater.* **2020**, *32*, 5854–5863.
[17] H. N. Nong, T. Reier, H.-S. Oh, M. Gliech, P. Paciok, T. H. T. Vu, D. Teschner, M. Heggen, V. Petkov, R. Schlögl, T. Jones, P. Strasser, *Nat. Catal.* **2018**, *1*, 841–851.
[18] Y. Wang, R. Ma, Z. Shi, H. Wu, S. Hou, Y. Wang, C. Liu, J. Ge, W. Xing, *Chem* **2023**, *9*, 2931–2942.
[19] a) C. Yang, X. Zhang, Q. An, M. Liu, W. Zhou, Y. Li, F. Hu, Q. Liu, H. Su, *J. Energy Chem.* **2023**, *78*, 374–380; b) P. C. Meenu, S. Roy, C. Chakraborty, S. Roy, *Adv. Powder Technol.* **2021**, *32*, 2663–2689.

Manuscript received: June 19, 2025
Revised manuscript received: August 4, 2025
Version of record online: ■■, ■■